Acta Astronautica 105 (2014) 444–462

Contents lists available at ScienceDirect

Acta Astronautica

journal homepage: www.elsevier.com/locate/actaastro

A six-degree-of-freedom hardware-in-the-loop simulator for small spacecraft

K. Saulnier [a], D. Pérez [b], R.C. Huang [a], D. Gallardo [a], G. Tilton [a], R. Bevilacqua [b,*]

[a] Department of Mechanical, Aerospace, and Nuclear Engineering, Rensselaer Polytechnic Institute (RPI), Troy, NY 12180, USA
[b] Department of Mechanical and Aerospace Engineering, University of Florida (UF), 308 MAE-A Building, P.O. Box 116250, Gainesville, FL 32611-6250, USA

ARTICLE INFO

Article history:
Received 26 December 2013
Received in revised form
25 August 2014
Accepted 17 October 2014

Keywords:
Small spacecraft
Hardware-in-the-loop verification
Guidance, navigation and control

ABSTRACT

This paper presents a novel six degree of freedom, ground-based experimental testbed, designed for testing new guidance, navigation, and control algorithms for the relative motion of nano-satellites. The development of innovative guidance, navigation and control methodologies is a necessary step in the advance of autonomous spacecraft. The testbed allows for testing these algorithms in a one-g laboratory environment. The system stands out among the existing experimental platforms because all degrees of freedom of motion are controlled via real thrusters, as it would occur on orbit, with no use of simulated dynamics and servo actuators. The hardware and software components of the testbed are detailed in the paper, as is the motion tracking system used to perform its navigation. A Lyapunov-based strategy for closed loop control is used in hardware-in-the loop experiments to successfully demonstrate the full six-degree-of-freedom system's capabilities. In particular, the test case shows a two-phase regulation experiment, commanding both position and attitude to reach specified final state vectors.

1. Introduction

The development of innovative guidance, navigation and control (GNC) strategies for relative spacecraft maneuvering will increase the efficiency and autonomy of future space missions [1]. Air bearing-based spacecraft simulators enable validation of GNC strategies prior to launch with hardware in the loop. Air bearings can provide near frictionless rotational and translational motion which can be utilized to create one-g laboratory conditions that are much closer to those encountered in a micro-gravity environment. Reference [2] provides a thorough review of air bearing based testbeds until the year 2003. The same paper also elaborates on how such testbeds have been developed over the last 50 years with the intention of validating GNC strategies for spacecraft, on the ground. A hardware-in-the-loop facility, enabling rapid prototyping of GNC algorithms for experimental testing, dramatically reduces the need for lengthy simulations every time (re-)tuning of the algorithms is performed. Ground testbeds can also support the advancement of the Technology Readiness Level (TRL) of spacecraft subsystems (see [3]).

Systems classified as only planar or only rotational are still widely used in on-the-ground testing. Examples of these include a rotational testbed at Georgia Tech, which is used for attitude matching experiments, and a planar testbed at Cornell University called FloatCube, which was created specifically for testing maneuvers of small scale cooperative satellites [4,5]. More complex systems combine

* Corresponding author. Tel.: +1 352 392 6230.
E-mail addresses: kniazx@gmail.com (K. Saulnier), davidperez777@msn.com (D. Pérez), astrorosemary@aol.com (R.C. Huang), daniele.gallardo@yahoo.it (D. Gallardo), tiltogv@gmail.com (G. Tilton), bevilr@ufl.edu (R. Bevilacqua).

http://dx.doi.org/10.1016/j.actaastro.2014.10.027
0094-5765/

Nomenclature

$\mathbf{A}$	error system matrix
$\mathbf{B}(\boldsymbol{\theta})$	error input matrix
$(\hat{\mathbf{b}}_x, \hat{\mathbf{b}}_y, \hat{\mathbf{b}}_z)$	body principal axis reference frame components
$\mathbf{C}(\boldsymbol{\theta})$	mapping from relative angular velocity to Euler angles
$\mathbf{e}$	combined rotation and translation error
$\mathbf{F}$	force vector
$\mathbf{G}(\boldsymbol{\theta})$	rotational input matrix
$\mathbf{H}$	thruster mapping matrix
$\mathbf{J}$	moment of inertia matrix
$\mathbf{K}$	reference model gain matrix
$\mathbf{M}$	moment vector
O	orbiting reference point
$\mathbf{P}$	Lyapunov matrix
$\mathbf{Q}$	positive definite matrix in Lyapunov equation
$\mathbf{R}(\boldsymbol{\theta})$	direction cosine matrix
$\mathbf{u}$	vector of thruster forces (N)
V	Lyapunov function
$(\hat{\mathbf{x}}, \hat{\mathbf{y}}, \hat{\mathbf{z}})$	LVLH frame components (mm)
$\boldsymbol{\epsilon}$	error vector between $\boldsymbol{\xi}$ and linear reference model
$\boldsymbol{\eta}$	collection of nonlinear terms
$\boldsymbol{\theta}$	2-1-3 Euler angle vector (rad)
$\boldsymbol{\nu}$	reference model input
$\boldsymbol{\xi}$	combined roto-translational displacement vector
$\boldsymbol{\rho}$	position vector relative to O (mm)
$\boldsymbol{\omega}$	angular velocity (rad/s)

Superscripts and subscripts

c	control input
F	associated with force
L	local vertical local horizontal frame
M	associated with moment
m	associated with reference model
S	spacecraft body fixed frame
x, y, z	x,y,z-component respectively
ρ	associated with translation
ω	associated with rotation

a planar translation stage and a rotational attitude stage to achieve five or six degrees of freedom. A five degree of freedom (5DOF) testbed has been developed by the Lawrence Livermore National Laboratory [6]. It combines a rotational platform with full freedom yaw, $\pm 15^\circ$ pitch and $\pm 30^\circ$ roll on a dynamic air bearing platform but does not have a vertical degree of freedom. More recent research related to 5DOF simulators has been done by Georgia Institute of Technology and Harbin Institute of Technology. Both projects combine a lower platform guaranteeing two translational degrees of freedom with an upper platform which uses a spherical air bearing, to provide an additional three rotational DOF [7,8]. An interesting example of a 6DOF testbed is the MIT "SPHERES" project [9,10]. This testbed can reach full 6DOF when used in the International Space Station (ISS)'s micro-gravity environment. However it can only achieve 3DOF on the ground with the assistance of a planar air bearing platform. 6DOF platforms have been developed by NASA Jet Propulsion Laboratory and New Mexico State University. In both cases the vertical motion giving the 6th degree of freedom is provided by a powered vertical system, which is actively controlled to provide a simulated zero-g environment for the attitude stage (AS) [11,12]. Reference [13] describes one of the most recent facilities reproducing 3DOF spacecraft relative motion in Italy, still under development. Reference [14] provides interesting observations on the benefits and need to develop and test algorithms on the ground with experimental platforms before actual flight. Other examples of 3DOF simulation facility testbeds can be found at the Naval Postgraduate School, looking at the different generations of robots utilized in the Spacecraft Robotics Laboratory [15,16]. The Distributed Space Systems Laboratory at Technion presents an interesting 3DOF system powered by ducted fans instead of compressed air thrusters, and floating thanks to a very specialized "hockey table".[1] A recent use of air bearing based testbeds focuses on validation of contact dynamics, to calibrate the algorithms and tools used in spacecraft servicing, refueling and assembly.[2] A different ground testing approach consists in employing robotic arms in conjunction with numerically simulated dynamics. Software integrates the equations of motion and those command the motion of servo actuators. This is a limited testing capability, where algorithms are validated with no use of real, space-like actuators. On the other hand, this approach enables the full 6DOF simulation with hardware-in-the-loop, at least for partial validation of subsystems like vision based navigation systems (see, for example, reference [17]).

This paper presents the 6DOF spacecraft simulator developed at the ADvanced Autonomous MUltiple Spacecraft laboratory. To the authors' knowledge, the presented system is the first reproducing all degrees of motion using real thrusters, without simulated dynamics and servo actuators used, for example, in the testbeds in References [11,12]. The goal of this work is to present the key characteristics of the ADAMUS testbed, and show its capabilities through an experimental test. Shown in Fig. 1, the ADAMUS testbed is similar to other 5 and 6DOF testbeds, which integrate the capabilities of planar systems and rotational systems. It differs from the existing 6DOF systems because it guarantees a realistically actuated motion along/about the full 6DOF. The motion in the vertical direction is accomplished using a unique method that employs a matched variable-mass counterbalance to the attitude stage (AS) and near-frictionless air bearing pulleys to allow close to gravity-free motion. The counterbalance system replaces

[1] http://dssl.technion.ac.il/
[2] http://ssco.gsfc.nasa.gov/index.html

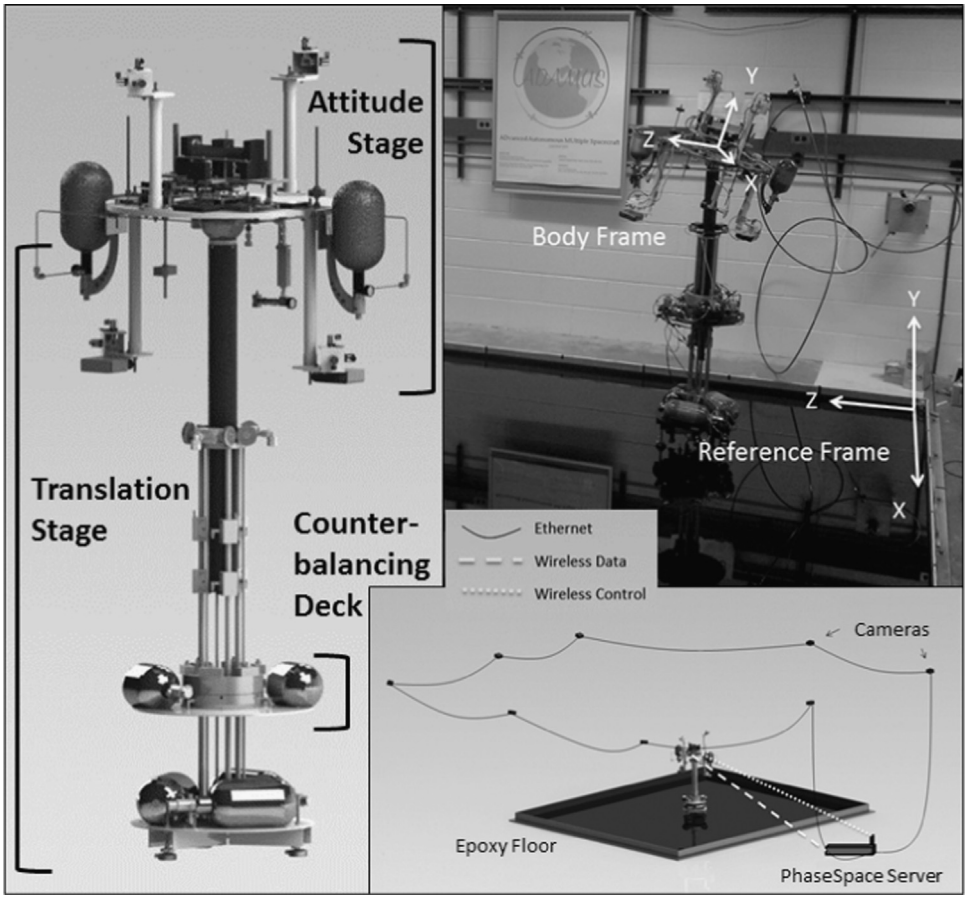

Fig. 1. ADAMUS testbed.

the powered vertical stages of other 6DOF testbeds and allows for control of all 6DOF using only the onboard thrusters. The resulting behavior of the system is much closer to the actual dynamics of satellites in space, as compared to systems that use linear motors or other solutions based on numerically modeling the vertical motion.

The design of the ADAMUS platform potentially allows for testing different spacecraft below 10 kg by switching out the AS. Fig. 1 shows the interchangeable AS, connected to the testbed base through the spherical air bearing. An additional restriction is given by the presence of the vertical pedestal, limiting the motion on two rotation axes, depending on the outer shape of the spacecraft.

The foremost contributions reported in this paper are:

1. Presentation of the ADAMUS 6DOF testbed hardware, reproducing a spacecraft motion controlled via thrusters only.
2. Implementation of a Lyapunov-based thruster activation control system on the 6DOF testbed for translational and rotational motions.
3. Demonstration of the capabilities of the 6DOF testbed for validating GNC algorithms for spacecraft performing autonomous maneuvers via hardware in the loop experiments.

This work is organized as follows: Section 2 gives an overview of the 6DOF testbed hardware, Section 3 illustrates the navigation method and supporting hardware used for the experiments, Section 4 describes the implemented Lyapunov-based thrusters' controls system, Section 5 explains the automatic generation of code from Simulink models used to program the onboard computer, and the results of GNC experiments that were performed on the 6DOF testbed. Section 6 presents the conclusions.

2. Testbed hardware

2.1. General overview

The testbed, shown in Fig. 1, is composed of a translational stage (TS), which was designed by the ADAMUS lab and built by Guidance Dynamics Corporation® (GDC) and an attitude stage, designed and built at the ADAMUS lab. The overall system operates on a flat epoxy surface. The position and attitude of the testbed is provided in real time by the PhaseSpace Impulse System® (PhaseSpace System), illustrated in the lower right picture in Fig. 1. The PhaseSpace System is a third party motion capture system, which streams tracking navigation data to the testbed's onboard computer.

The AS represents the satellite and contains the subsystems required for the GNC to be tested. These subsystems include an onboard PC104 computer, thrusters, navigation components, and fuel. The AS is connected to the TS via a spherical air bearing, which allows for low friction rotational motion of the AS. The TS facilitates translation of the AS. For vertical motion, a system of air pulleys on the TS connects the central column and AS to a counterbalancing deck (CD) with a matching mass. The mass of the CD compensates for the mass of the AS to allow for gravity-free motion. For translation in the other two degrees of freedom, three linear air bearings create an air cushion between the TS and a 13 ft × 15 ft epoxy floor, allowing the TS to translate with very little friction. The epoxy floor was built by Precision Epoxy Products, a division of Rock Art, Ltd. The TS also carries the compressed air required to run all of the air bearings in the testbed. Further details on the TS and AS are provided in the following sections.

2.2. Translational stage

The function of the TS is to provide the 3 translational degrees of freedom. The two horizontal degrees of freedom are provided by linear air bearings, which create an air cushion to separate the structure from the epoxy floor, allowing for nearly friction free motion. Hanging on the structure of the TS is the counterbalancing system that provides the third translational degree of freedom. This system will be further detailed in Section 2.3.

The main structure of the TS was custom built by Guidance Dynamics Corporation®, according to the ADAMUS laboratory design. Fig. 2 shows a rendering alongside the actual TS. Table 1 provides a list of the main components of the TS and their sources.

The TS also carries the compressed air tanks and pneumatics that store and distribute the air used by all the air bearings and air bushings of the platform. The pneumatic system of the translational stage is shown in Fig. 3.

In this diagram, each “Tank” is a 4500 psi paintball tank as listed in Table 1. The tanks are connected in parallel to three separate regulators that step down the tank pressures to 100 psi, 90 psi, and 30 psi. At the output of each regulator there is a valve that is controlled manually to turn the air flow on or off to each of the air bearing subsystems. One valve controls the connection of a 100 psi line that connects to the linear air bearing feet. A separate valve is used to connect a 90 psi line to a set of bushings that are involved in guiding the counterbalance system. Lastly, a third valve connects a 100 psi line to the spherical cup air bearing that supports the spherical segment ball attached to the AS.

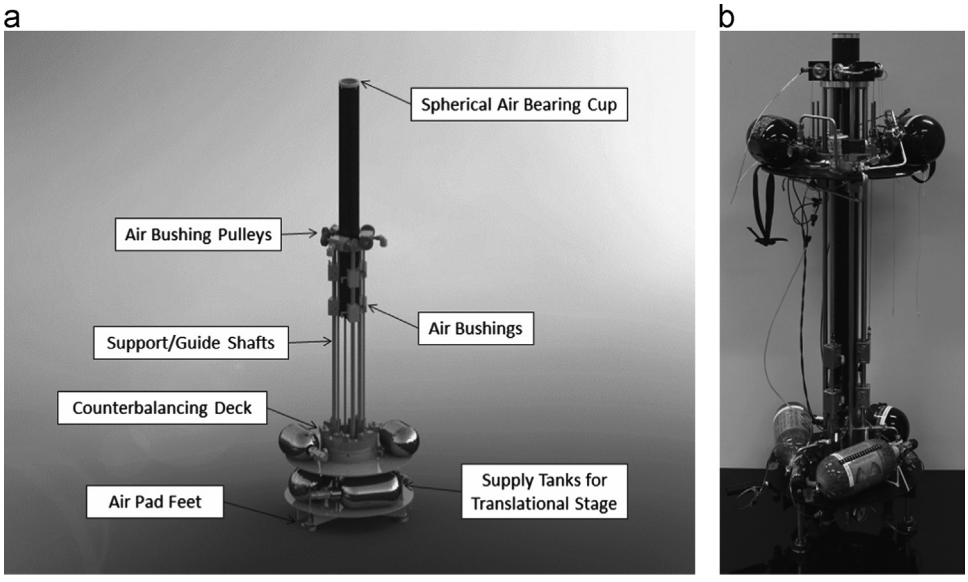

Fig. 2. Translational stage. (a) Rendered and (b) actual.

Table 1
Components of translational stage.

Component	Model number	Company
Platform	Custom	Guidance Dynamics Corporation
4500 psi, 70cu Paintball Air Tanks, 3x	Pure Energy P11G-001	Luxfer
Regulators, 3x	969	Aqua Environment
Hand Valve, 3x	104104-N01	Ingersoll Rand
Stabilizer	PPSP01190*	Palmers
Flat Round Air Bearings, 3x	S105001	Newway

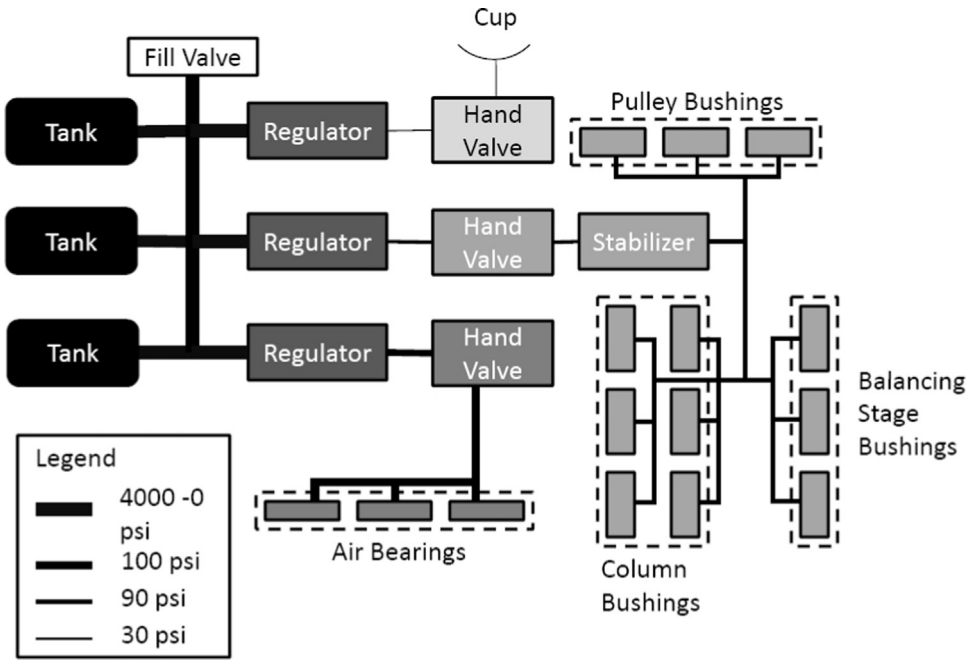

Fig. 3. Translational stage pneumatics.

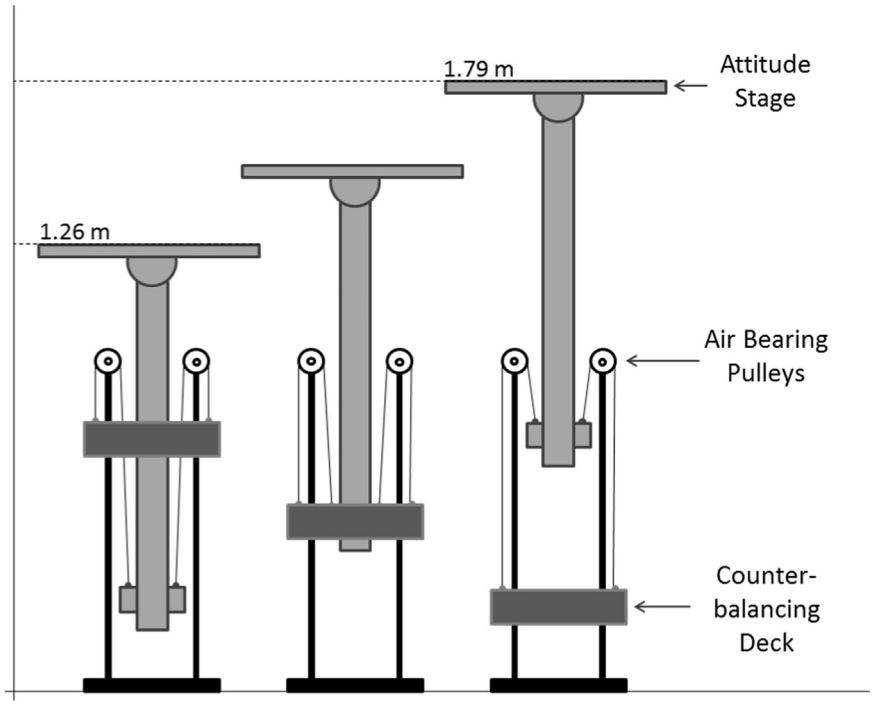

Fig. 4. Counterbalancing concept.

2.3. Counterbalancing system

The vertical degree of freedom is provided by a counterbalancing system consisting of a counterbalancing deck of the same mass as the AS and supporting column. Fig. 4 contains a diagram of the counterbalancing concept with the minimum and maximum heights reached by the AS.

The deck and central column are connected via an air bearing pulley system. The counterbalance motion is guided by two sets of vertical bars attached to the TS. One set of bars guides and stabilizes the CD, which is connected to the bars using air bushings. The other set of bars guides and supports the central column, and by extension the AS, via another set of air bushings.

The guides also serve to prevent collisions between the closely moving parts. The air bushings used in the pulley system and for the guides are supplied with air from the TS tanks as illustrated in Fig. 3. Flexible tubing is used to bring the air to the counterbalancing system without interfering with its motion. Table 2 contains all the major components used in the counterbalancing system and the CD is shown in Fig. 5a.

During an experiment, the mass of the CD is changed to compensate for the AS mass lost as air is released through the thrusters. In order to maintain the zero gravity effect on the AS motion it is important to maintain the balance in the counterbalance system. Although the CD and AS can be balanced using static weights before each experiment, the AS can change mass by up to 300 g as the experiment is run and the air in its tanks is depleted. To reduce this disturbance to manageable levels, the CD also releases air from its two tanks during each experiment. The associated pneumatic system is shown in Fig. 5b. The release of air is controlled by an Arduino Uno, which receives pressure readings from the AS tanks from the PC104 over WiFi via the WiFly expansion board. A reading is then taken from the CD tanks using a pressure transmitter and the two values are compared. If the value received from the AS is lower, the Arduino opens a magnetic latching valve, which vents air from the tanks that have been reduced in pressure to 80 psi using a regulator. The valve remains open to release air from the CD until the pressures are equalized. If the value received from the AS is higher or equal, no air is released. Through this method, the pressure in the AS and CD tanks remains equal within a margin of ± 50 psi, as dictated by the precision of the pressure

Table 2
Components of counterbalance system.

Component	Model number	Company
Platform	Custom made	Guidance Dynamics Corporation
Pulley Bushing, 3x	S301901	Newway
Pulley Bushing Mounting Block, 3x	S8019P02	Newway
CD Guide Bushing, 3x	S301201	Newway
CD Guide Bushing Mounting Block, 3x	Custom	D & K
Column Air Bushings, 6x	S301201	Newway
Column Bushing Mounting Block, 6x	Custom	D & K
Pulleys	D 1796	Prime-Line
4500 psi, 50cu Paintball Air Tanks, 2x	Carbon Fiber N2	Ninja
Regulator	969	Aqua environment
Pressure Sensor	A-10	WIKA
Solenoid Valve	23KK7DELM	Peter Paul Electronics
Computer	Uno	Arduino
Wireless Connector	WiFly	Roving Networks
Solenoid Battery, 2x	UBBL20-FL	ULTRALiFE
Arduino Battery	RLI-9600	HiTECH

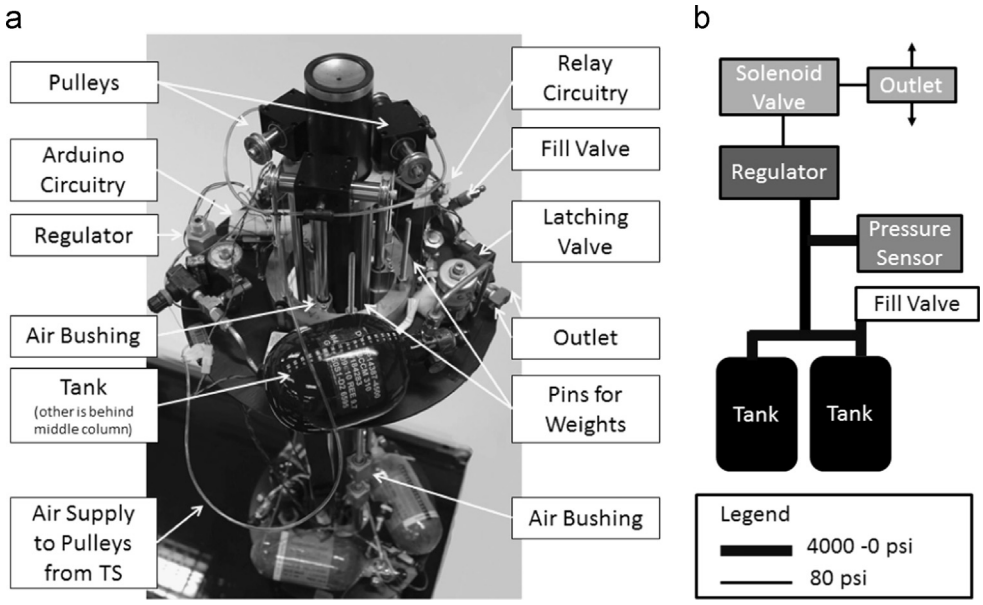

Fig. 5. Counterbalancing system. (a) Deck, pulleys, and bushings and (b) pneumatics scheme.

transmitters used. Air from the CD is released from a T joint to prevent the released air from affecting the movement of the counterbalancing system or TS in general. The limitations of this method are covered further in Section 5.4

The electrical system on the CD consists of a pressure transducer, Arduino Uno, WiFly expansion board, magnetic latching valve, and a diode and relay circuit that shields the Arduino and allows it to control the current supplied to the valve. The system is powered by a 9 V battery with the exception of the valve, which has a separate 6 V source. The Arduino reads the pressure of the CD tanks from the pressure transducer through an A/D port and compares it to the pressure of the AS tanks, which is received wirelessly from the PC104 using the WiFly board. The Arduino controls the release of air using digital I/O ports and a relay circuit. The two states of the relay circuit which are used, control the direction of current received by the magnetic latching valve. This circuit can be seen in Fig. 6. In one state, the current received is such that the valve opens, releasing air. In the other the current is reversed, so the valve closes and the release of air is stopped.

2.4. Attitude stage

The AS represents the satellite and provides the three rotational degrees of freedom of the testbed. The rotational degrees of freedom are provided by a spherical air bearing, shown in Fig. 7, which serves to connect the AS to the TS central column.

Fig. 8 shows the AS detached from the TS in a front and top view respectively.

In addition, the major pneumatic and electrical components of the AS are listed in Table 3.

The AS is composed of a disc made of composite material (fiber glass and high density foam) connected to the spherical air bearing. Attached to the AS are four arms made of ABS and PVC. Two arms extend upwards and the other two arms extend downwards. The arms are attached symmetrically to the disc to facilitate mass balancing and to provide a symmetric thruster layout. There are three thrusters mounted orthogonally on the end of each arm. Using a unique combination of active thrusters it is possible to obtain independent translational and/or rotational motions. The AS provides full 360° freedom in yaw but the structure limits it to $\pm 30^{\circ}$ about the pitch and roll axes.

The pneumatic system of the AS, illustrated in Fig. 9, is used to supply air to the thrusters, which control the motion of the testbed. Thruster fuel in the form of compressed air is stored in two carbon fiber paintball tanks attached to the AS. The tanks are connected in parallel to a regulator, which steps the pressure down to 165 psi before it is distributed to the thrusters. The thrusters, shown in Fig. 8b, consist of solenoid valves attached to custom made nozzles. Over the course of an experiment, mass is lost from the tanks as air is released from the thrusters. By connecting the tanks in parallel and by aligning the center of mass of the tanks with the center of mass of the AS, the change in mass does not affect the overall balance of the AS. A pressure transmitter is connected before the regulator to allow the PC104 to receive measurements of the pressure left in the tanks. The pressure readings are used in the counterbalancing system as described in Section 2.3.

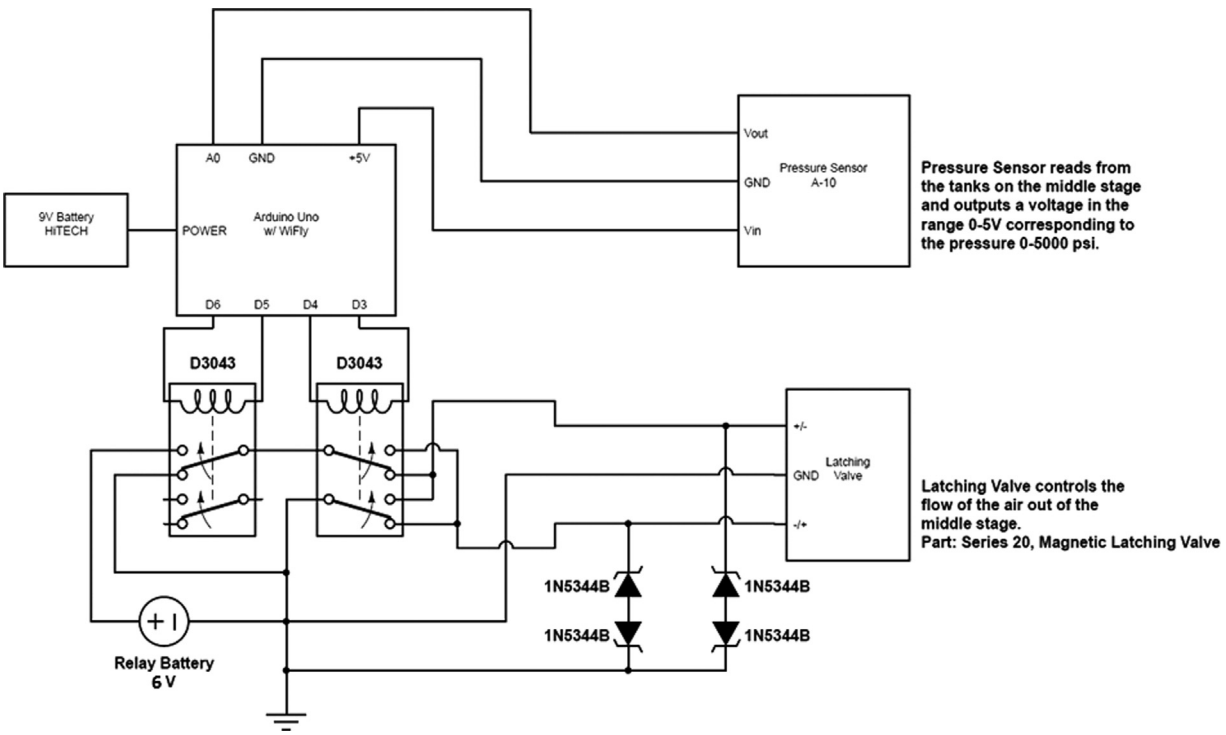

Fig. 6. Counterbalancing deck electrical.

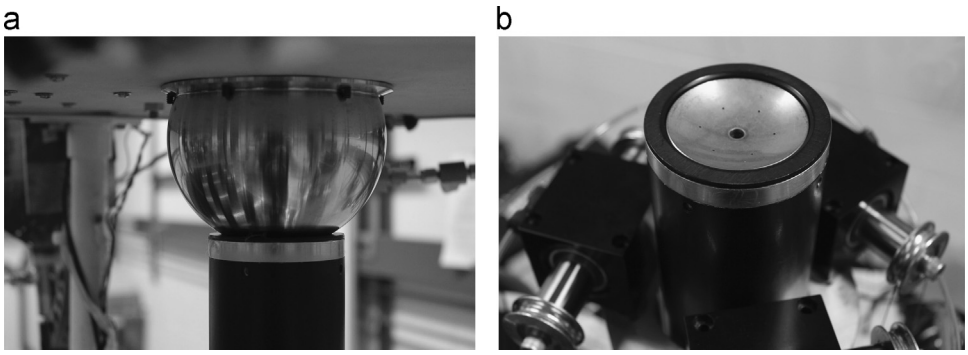

Fig. 7. Spherical bearing. (a) Bearing and (b) cup.

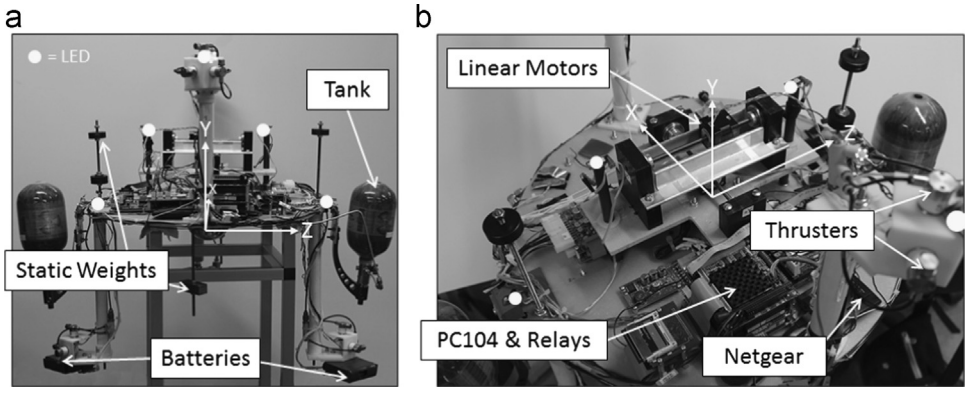

Fig. 8. Attitude stage. (a) Front and (b) top.

Table 3
Components of attitude stage.

Component	Model Number	Company
Platform	Custom	ADAMUS lab.
Spherical Bearing	Custom	D & K
4500 psi, 50cu Paintball Air Tanks, 2x	Pure Energy P07B-001	Luxfer
Regulator	1247-2	Aqua Environment
Solenoid Valve, 12x	EH2012	Gems Sensors
Thrusters	12-056	Gordon Engineering
Pressure Sensor	A-10	WIKA
PC/104 Computer	ADLS15PC	ADL Embedded Solutions
PC/104 Relay Board	IR-104	Diamond Systems
PC/104 I/O Module	DMM-32DX-AT	Diamond Systems
Motion Control Card	DMC-2133	Galil Motion Control
Motor Driver Board	SDM-20242	Galil Motion Control
DC-ATX Converter	DC123SR	OceanServer
DC-DC Step-Up Converter	DC1U-1VR	OceanServer
Battery Management Module	BB-04SR	OceanServer
Battery Pack, 2x	BA95HC-FL	OceanServer
Wireless Receiver	WNCE2001	Netgear
AS Balancing Motors	35F4N-2.33-024	Haydon Kerk
AS Balancing Platform Motor	35H4N-2.33-049	Haydon Kerk

The flat disk of the AS also supports some components of the PhaseSpace System, the on-board computer, wireless receiver, and a balancing system. A diagram detailing the AS electrical system and its connections to the other systems in the testbed is provided in Fig. 10. The on-board portion of the PhaseSpace system consists of a string of six LEDs and a device called the "puck." The puck controls the power to the LEDs, which are necessary for the PhaseSpace System to determine the state of the AS. The PhaseSpace LEDs are positioned on the edges of the arms and on the middle of the upper platform.

Central to the electrical system on the AS is an Advanced Digital Logic ADLS15PC Rev. 1.3 computer (PC104), which

runs Real-Time Application Interface (RTAI) Linux. The PC104 in turn is connected to an I/O board and a relay board, which allow it to obtain pressure readings from the tanks and to control the thruster valves according to the current GNC algorithm. The PC104 is also able to control a motor driver and motor controller card, which are used in the balancing system of the AS. The PC104 is controlled wirelessly from an off-board desktop computer by means of a Netgear wireless receiver. The same receiver is then used during experiments to communicate with both the off-board components of the PhaseSpace System and the Arduino Uno on the CD.

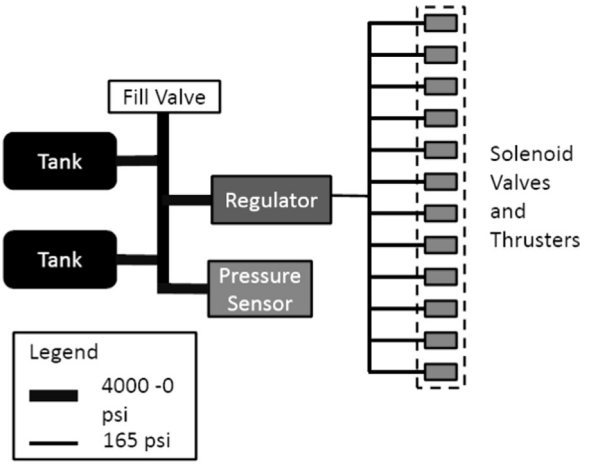

Fig. 9. Attitude stage pneumatics.

All of the AS electrical subsystems, except the PhaseSpace puck and LEDs, rely on 2 lithium-ion batteries for power. The batteries are situated on the lower arms to help compensate for the mass of the systems above the disk. These batteries are connected to a Power Management System from Ocean Server Technology (IBPS: Intelligent Battery and Power System). The IBPS recharges the batteries when connected to the 120 V grid using a safety charging circuit, and provides power to the AS subsystems at several voltages. The IBPS provides 5 V power to the PC104 and 12 V power to a separate 12 V to 24 V DC–DC converter. The IBPS also provides power to the motor driver and motor controller card. The 12 V to 24 V DC–DC converter outputs 24 V to the thrusters through the relay board controlled by the PC104.

An important consideration when dealing with rotational testbeds is that the center of mass and center of rotation must be co-located to eliminate gravity torques. The center of rotation of the AS is located in the center of the spherical air bearing that connects it to the TS. Rough balancing is performed with static weights placed in four locations around the AS platform, as shown in Fig. 8a. Although the AS can be completely balanced using the static weights, the movement of small masses, such as wires and the small changes of position of parts, which are

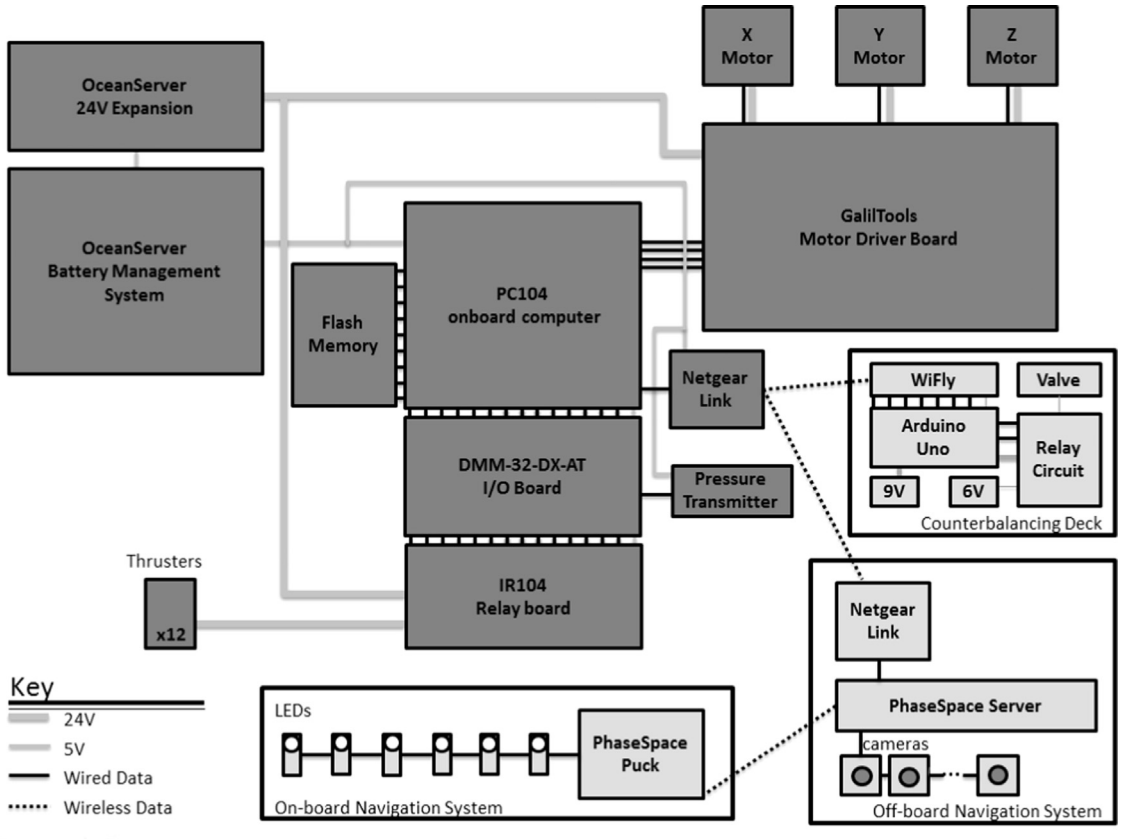

Fig. 10. Attitude stage electronics connections and signals.

removed for charging and repairs can shift the center of mass between experiments. To deal with small misalignment in the center of mass and center of rotation, a fine active mass balancing system called the balancing platform (BP) is also present on the AS. The BP consists of three linear motors, which translate along the three body axes, shown in Fig. 8b. The motor's translation causes a shift in the center of mass of the AS. Current balancing techniques are human-in-the-loop with the motors controlled via a motor driver board with a serial connection to the onboard computer. Before each experiment, the masses are moved incrementally until the AS does not move when placed in several angled configurations. Since the balancing is done human-in-the-loop, this does not remove all disturbances from gravity torques; it serves to reduce the effects to a disturbance easily overcome by the thrusters. Controlling the alignment electronically also opens the door to alignment using adaptive methods [18,19]. When implemented, automatic methods will provide a more finely and consistently balanced AS.

3. Testbed navigation and attitude determination

The navigation of the testbed is accomplished using a PhaseSpace Impulse System®. The PhaseSpace System (which is further explained below) outputs a state vector that contains the position of the AS in millimeters, relative to a coordinate frame positioned at one of the corners of the epoxy floor, and quaternions representing the attitude of the AS. The error has been calculated in [20] to be 1–5 mm with a mean latency of 8 ms. This data is sent wirelessly to the PC104 where an executable real time program uses it to generate the linear and angular velocities of the AS using a Kalman filter and extended Kalman filter, respectively.

The PhaseSpace System is a third party system that consists of a set of cameras mounted on the walls around the test area, a set of red LEDs mounted on the object to be tracked, and a server which runs the proprietary software from PhaseSpace Inc. The system is easily configurable and can be set up to track new objects without excessive calibration or data post-processing. The PhaseSpace server comes equipped with a software suit which includes C++ libraries to which can be used to make the data available to other applications. The ADAMUS lab used those libraries to create S-functions which allow the position and attitude data collected by the PhaseSpace software to be accessed by MATLAB in Simulink and by real time executables created using the Simulink Coder [21].

3.1. Hardware

The PhaseSpace hardware consists of an on-board LED system and an off-board data collection system. The onboard system consists of a small rechargeable battery pack and a string of LED circuits. On the testbed the LED string consists of 6 LED circuits positioned around the AS, but the PhaseSpace System can be configured to track as many as 72 LEDs which could be used to define a nonrigid AS structure. Fig. 11 shows the distribution of LEDs on the AS.

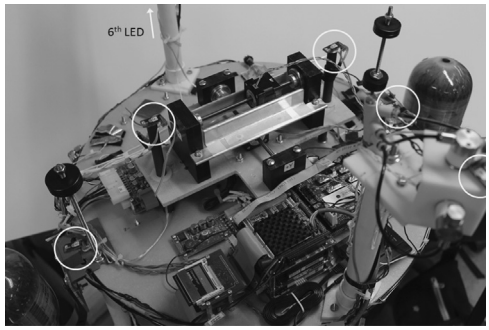

Fig. 11. Positions of LEDs on AS indicated with white circles.

Each LED circuit contains a red LED which blinks rapidly in a unique pattern. To conserve power, the battery pack is wirelessly controlled to go to a low power state when the system is not in use. The off-board system consists of a dedicated server computer provided by PhaseSpace, Inc., which communicates over Ethernet with each of a set of 8 PhaseSpace cameras posted around the epoxy floor, as illustrated in Fig. 1. The cameras pick up the blinking LEDs and that data is used by the server to determine position and attitude of the AS, which can be transmitted to the PC104 with a latency of 8 ms and precision of 1–5 mm.

3.2. Software

The testbed uses a C++ communications library provided by PhaseSpace, Inc. to allow the PC104 to request data from the PhaseSpace. The PhaseSpace Server comes preloaded with software which is used to configure the tracking program. In order to determine the attitude and position of an object equipped with PhaseSpace LEDs, the system must be configured using the PhaseSpace software. This configuration process assigns the location of the origin in the cameras' field of view as well as the orientation of the AS which corresponds to zero attitude. After the one time configuration is performed, an S-function developed in the lab can be used to acquire real time position and attitude measurements. The S-function outputs a single 7-element vector of the position and quaternion for the tracked object, as calculated by the PhaseSpace server. Fig. 12 shows the steps taken to acquire position and attitude data.

The position data is processed through a Kalman filter in order to estimate the position and velocity. An extended Kalman filter processes the measured attitude data to estimate the attitude of the AS. The angular velocity data is computed using a discrete derivative of the filtered attitude data, which is passed through a low pass filter to decrease noise. The filter is chosen to balance the speed of the filter and the noise rejection. It is important to mention that a different AS, with a different actuation system, and different GNC software could be used, provided that this software can interact with the PhaseSpace system.

4. Lyapunov controller for thrusters

The control strategy, chosen to demonstrate the testbed's capabilities, is adapted from the Lyapunov thruster

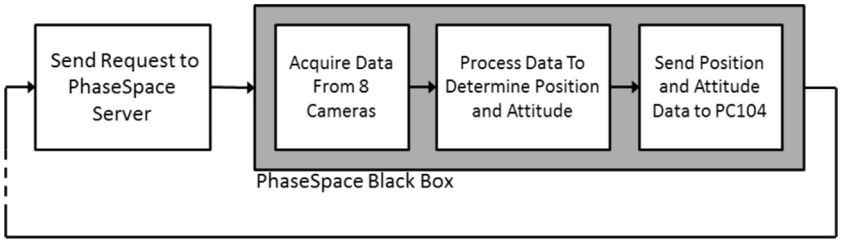

Fig. 12. Flowchart showing the basic steps to acquire position and attitude data.

selection approach described in [22]. The active thrusters are chosen at each time step to maintain a negative derivative to a Lyapunov function created with a linear reference model, thus ensuring stability of the tracking error. The Lyapunov method of selecting thrusters eliminates the need for thruster mapping and provides a computationally simple, and non-iterative, method for 6DOF control of a spacecraft.

4.1. Dynamics

The equations of relative motion for a spacecraft are developed from the local-vertical-local-horizontal (LVLH) frame $(\hat{\mathbf{x}}, \hat{\mathbf{y}}, \hat{\mathbf{z}})$ attached to an orbiting reference point O, where the $\hat{\mathbf{x}}$ axis points in the radial direction from the center of the attracting body to the spacecraft, the $\hat{\mathbf{y}}$ points along the local horizon in the direction of motion of O, and $\hat{\mathbf{z}}$ points in the direction $\hat{\mathbf{x}} \times \hat{\mathbf{y}}$. Another reference frame that will be used is the spacecraft body principal axis reference frame (body frame) $(\hat{\mathbf{b}}_x, \hat{\mathbf{b}}_y, \hat{\mathbf{b}}_z)$, which can be seen in Figs. 1 and 8.

If the reference point O is assumed to be in a circular orbit, and the relative distance of the spacecraft from O is significantly smaller than the orbital radius, then the Hill–Clohessy–Wiltshire linear equations describe the translational motion [23]. They are

$$\begin{aligned} \ddot{x} &= 3n^2x + 2n\dot{y} + \frac{1}{m}{}^{L}F_{cx} \\ \ddot{y} &= -2n\dot{x} + \frac{1}{m}{}^{L}F_{cy} \\ \ddot{z} &= -n^2z + \frac{1}{m}{}^{L}F_{cz} \end{aligned} \tag{1}$$

where n is the mean motion, x, y, and z are the components of the relative position in the LVLH frame, and ${}^{L}F_{cx}$, ${}^{L}F_{cy}$, and ${}^{L}F_{cz}$ are the components of the control forces in the LVLH frame. For the case where a spacecraft is maneuvering very close to O and the maneuvers duration is much shorter than the orbital period, the coupling terms can be ignored, then the relative translational motion can be approximated by

$$\ddot{\boldsymbol{\rho}} = \frac{1}{m}{}^{L}\mathbf{F}_c \tag{2}$$

where $\boldsymbol{\rho} = [x\ y\ z]^{\top}$ and ${}^{L}\mathbf{F}_c = [{}^{L}F_{cx}\ {}^{L}F_{cy}\ {}^{L}F_{cz}]^{\top}$. For the maximum relative positions (4 m and 4.5 m in the plane, 0.56 m in the vertical direction) and velocities (starting approximately from rest) achievable with the platform, the coupling terms are at least one order of magnitude smaller than the remaining terms in the right-hand side of Eq. (1) for orbits with a radius of at least 6041.4 km. This value is below the mean radius of the Earth (6378.1 km); hence, this assumption is reasonable for any physically realizable orbit about the Earth.

In this case, the translational dynamics closely matches that of the ADAMUS 6DOF testbed. Eq. (2) is what is used to develop and test controllers on the testbed.

The controller presented in this paper uses rotational equations of motion developed from 2-1-3 Euler angle representation of the attitude of a spacecraft body frame relative to the LVLH frame. In the case of the testbed, the LVLH frame is the frame fixed to the epoxy floor and corresponds with the PhaseSpace object coordinate frame. The rotational kinematics of the body frame relative to the LVLH in terms of 2-1-3 Euler angles

$$\dot{\boldsymbol{\theta}} = \mathbf{C}(\boldsymbol{\theta})[\boldsymbol{\omega}_S - {}^{S}\mathbf{R}_L(\boldsymbol{\theta})\boldsymbol{\omega}_L] \tag{3}$$

where $\boldsymbol{\theta} = [\theta_x\ \theta_y\ \theta_z]^{\top}$ has the Euler angles reordered into a vector, $\boldsymbol{\omega}_S$ is the inertial angular velocity expressed in terms of the body fixed principal axes of inertia of the spacecraft, which define the S frame, $\boldsymbol{\omega}_L$ is the inertial angular velocity of the LVLH frame. ${}^{S}\mathbf{R}_L(\boldsymbol{\theta})$ is the direction cosine matrix from the LVLH frame to the S frame which is

$${}^{S}\mathbf{R}_L(\boldsymbol{\theta}) = \begin{bmatrix} c_zc_y + s_zs_xs_y & s_zc_x & -c_zs_y + s_zs_xc_y \\ -s_zc_y + c_zs_xs_y & c_zc_x & s_zs_y + c_zs_xc_y \\ c_xs_y & -s_x & c_xc_y \end{bmatrix} \tag{4}$$

where $c_x := \cos(\theta_x)$, $s_x := \sin(\theta_x)$, $c_y := \cos(\theta_y)$, $s_y := \sin(\theta_y)$, $c_z := \cos(\theta_z)$, and $s_z := \sin(\theta_z)$. $\mathbf{C}(\boldsymbol{\theta})$ is the mapping from the relative angular velocity to the rates of change of the Euler angles, and in this case it is

$$\mathbf{C}(\boldsymbol{\theta}) = \begin{bmatrix} c_z & -s_z & 0 \\ s_z/c_x & c_z/c_x & 0 \\ s_zt_x & c_zt_x & 1 \end{bmatrix} \tag{5}$$

where $t_x := \tan(\theta_x)$.

For a rigid body, the rotational dynamics is

$$\dot{\boldsymbol{\omega}}_S = \mathbf{J}^{-1}(-[\tilde{\boldsymbol{\omega}}_S]\mathbf{J}\boldsymbol{\omega}_S + {}^{S}\mathbf{M}_c) \tag{6}$$

where J is principal moments of inertia matrix, ${}^{S}\mathbf{M}_c$ is the vector of control torques in the S frame, and $[\tilde{\boldsymbol{\omega}}_S]$ is a skew symmetric matrix representing the cross product operation in matrix form. That is,

$$[\tilde{\boldsymbol{\omega}}_S] = \begin{bmatrix} 0 & -\omega_z & \omega_y \\ \omega_z & 0 & -\omega_x \\ -\omega_y & \omega_x & 0 \end{bmatrix} \tag{7}$$

where ω_x, ω_y, and ω_z are the components of $\boldsymbol{\omega}_S$. Rearranging Eq. (3) an expression for the angular velocity of the

spacecraft can be obtained as

$$\boldsymbol{\omega}_S = \mathbf{C}^{-1}(\boldsymbol{\theta})\dot{\boldsymbol{\theta}} + {}^S\mathbf{R}_L(\boldsymbol{\theta})\boldsymbol{\omega}_L \tag{8}$$

A second-order set of differential equations governing the evolution of the 2-1-3 Euler angles can be obtained by taking the derivative of (3) and using (6) and (8):

$$\ddot{\boldsymbol{\theta}} = \mathbf{f}(\boldsymbol{\theta}, \dot{\boldsymbol{\theta}}, \boldsymbol{\omega}_L, \dot{\boldsymbol{\omega}}_L) + \mathbf{G}(\boldsymbol{\theta}){}^S\mathbf{M}_c \tag{9}$$

where $\mathbf{G}(\boldsymbol{\theta}) \coloneqq \mathbf{C}(\boldsymbol{\theta})\mathbf{J}^{-1}$ and $\mathbf{f}(\boldsymbol{\theta}, \dot{\boldsymbol{\theta}}, \boldsymbol{\omega}, \dot{\boldsymbol{\omega}})$ is a nonlinear vector function. With $\boldsymbol{\omega}_L = 0$ and $\dot{\boldsymbol{\omega}}_L = 0$ as in the laboratory fixed reference frame, these become the equations of motion used for the attitude control of the testbed.

$$\ddot{\boldsymbol{\theta}} = \mathbf{f}(\boldsymbol{\theta}, \dot{\boldsymbol{\theta}}) + \mathbf{G}(\boldsymbol{\theta}){}^S\mathbf{M}_c \tag{10}$$

Due to the fact that thrusters are being used to control the testbed, the attitude and translational control are coupled, and thus ${}^S\mathbf{M}_c$ and ${}^L\mathbf{F}_c$ must be designed together [22]. It is also necessary to determine the contribution of each thruster to ${}^S\mathbf{M}_c$ and ${}^L\mathbf{F}_c$. With this in mind, first define a vector of thruster forces for each thruster as $\mathbf{u} = u[\hat{u}_1\ \hat{u}_2 \cdots \hat{u}_n]^\top$ where

$$\hat{u}_i = \begin{cases} 0 & i\text{th thruster off} \\ 1 & i\text{th thruster on} \end{cases} \quad i = 1, 2, \ldots, n \tag{11}$$

and u is the magnitude of the thrust a single thruster produces.

The forces and moments in the body frame can be calculated by

$$\begin{bmatrix} {}^S\mathbf{F}_c \\ {}^S\mathbf{M}_c \end{bmatrix} = \begin{bmatrix} \mathbf{H}_F \\ \mathbf{H}_M \end{bmatrix} \mathbf{u} = \mathbf{H}\mathbf{u} \tag{12}$$

where $\mathbf{H}$ is a matrix that maps the vector of thrusts $\mathbf{u}$ to the forces and moments in the body frame, which are written as ${}^S\mathbf{M}_c$ and ${}^S\mathbf{F}_c$. The submatrices $\mathbf{H}_F$ and $\mathbf{H}_M$ individually map $\mathbf{u}$ to ${}^S\mathbf{F}_c$ and ${}^S\mathbf{M}_c$, respectively. ${}^S\mathbf{F}_c$ are the input forces in the S frame and can be found using ${}^S\mathbf{F}_c = {}^S\mathbf{R}_L(\boldsymbol{\theta}){}^L\mathbf{F}_c$. $\mathbf{H}$ is determined based on how the thrusters are physically laid out on the AS. In this case the thrusters are configured as shown in Fig. 13, which results in the following matrices:

$$\mathbf{H}_F = \begin{bmatrix} c & -c & 0 & c & c & 0 & -c & -c & 0 & -c & c & 0 \\ 0 & 0 & 1 & 0 & 0 & -1 & 0 & 0 & -1 & 0 & 0 & 1 \\ c & c & 0 & c & -c & 0 & -c & c & 0 & -c & -c & 0 \end{bmatrix} \tag{13}$$

$$\mathbf{H}_M = \begin{bmatrix} -c & -c & 0 & c & -c & 0 & -c & c & 0 & c & c & 0 \\ -0.5 & 0.5 & 0 & 0.5 & -0.5 & 0 & 0.5 & -0.5 & 0 & -0.5 & 0.5 & 0 \\ c & -c & 0 & -c & -c & 0 & c & c & 0 & -c & c & 0 \end{bmatrix} d \tag{14}$$

where d is the moment arm and $c = 0.7071$.

Let $\boldsymbol{\xi} \coloneqq [\boldsymbol{\rho}\ \boldsymbol{\theta}]^\top$ be the combined roto-translational displacement vector, then Eqs. (2), (10), and (12) can all be combined to produce the following coupled thruster commanded dynamics:

$$\ddot{\boldsymbol{\xi}} = \mathbf{p}(\boldsymbol{\xi}, \dot{\boldsymbol{\xi}}) + \mathbf{N}(\boldsymbol{\theta})\mathbf{H}\mathbf{u} \tag{15}$$

where

$$\mathbf{p}(\boldsymbol{\xi}, \dot{\boldsymbol{\xi}}) = \begin{bmatrix} \mathbf{0} \\ \mathbf{f}(\boldsymbol{\theta}, \dot{\boldsymbol{\theta}}) \end{bmatrix} \tag{16}$$

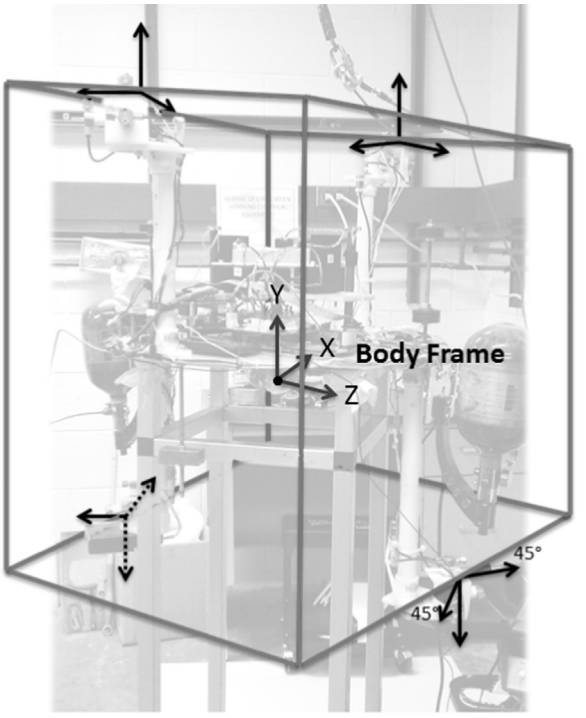

Fig. 13. Testbed thruster configuration.

and

$$\mathbf{N}(\boldsymbol{\theta}) = \begin{bmatrix} \frac{1}{m}{}^L\mathbf{R}_S(\boldsymbol{\theta}) & \mathbf{0} \\ \mathbf{0} & \mathbf{G}(\boldsymbol{\theta}) \end{bmatrix} \tag{17}$$

where ${}^L\mathbf{R}_S(\boldsymbol{\theta}) = {}^S\mathbf{R}_{LL}{}^\top(\boldsymbol{\theta})$.

4.2. Reference model tracking

The goal of the controller will be to follow $\boldsymbol{\rho}_m$ and $\boldsymbol{\sigma}_m$, which are defined as the solutions to the following linear reference models [22]:

$$\ddot{\boldsymbol{\rho}}_m + \mathbf{K}_1\dot{\boldsymbol{\rho}}_m + \mathbf{K}_2\boldsymbol{\rho}_m = \boldsymbol{\nu}_{\rho c} \quad \ddot{\boldsymbol{\theta}}_m + \mathbf{K}_3\dot{\boldsymbol{\theta}}_m + \mathbf{K}_4\boldsymbol{\theta}_m = \boldsymbol{\nu}_{\theta c} \tag{18}$$

where $\mathbf{K}_1$, $\mathbf{K}_2$, $\mathbf{K}_3$, and $\mathbf{K}_4$ are 3×3 symmetric positive definite matrices, and $\boldsymbol{\nu}_{\rho c}$ and $\boldsymbol{\nu}_{\theta c}$ can be thought of as input variables to the linear reference models. The values of $\boldsymbol{\nu}_{\rho c}$ and $\boldsymbol{\nu}_{\theta c}$ will determine the type of control problem. If $\boldsymbol{\nu}_{\rho c} = \mathbf{0}$ and $\boldsymbol{\nu}_{\theta c} = \mathbf{0}$ then tracking the linear reference model becomes a regulation problem; otherwise, $\boldsymbol{\rho}_m$ and $\boldsymbol{\sigma}_m$ are the responses of the second order system described in Eq. (18) to inputs $\boldsymbol{\nu}_{\rho c}$ and $\boldsymbol{\nu}_{\theta c}$.

In order to track the linear reference model Eq. (18), error variables between the linear reference model and the nonlinear dynamics are defined as $\boldsymbol{\epsilon}_\rho = \boldsymbol{\rho} - \boldsymbol{\rho}_m$ and $\boldsymbol{\epsilon}_\theta = \boldsymbol{\theta} - \boldsymbol{\theta}_m$. The controller is designed to drive the error system asymptotically to zero. Combining these error variables with Eqs. (2), (10), (12), and (18) result in the following equations governing the evolution of the error

$$\begin{aligned} \ddot{\boldsymbol{\epsilon}}_\rho + \mathbf{K}_1\dot{\boldsymbol{\epsilon}}_\rho + \mathbf{K}_2\boldsymbol{\epsilon}_\rho &= \frac{1}{m}{}^L\mathbf{R}_S(\boldsymbol{\theta})\mathbf{H}_F\mathbf{u} - \left(\boldsymbol{\nu}_{\rho c} - \boldsymbol{\eta}_{\rho l}\right) \\ \ddot{\boldsymbol{\epsilon}}_\theta + \mathbf{K}_3\dot{\boldsymbol{\epsilon}}_\theta + \mathbf{K}_3\boldsymbol{\epsilon}_\theta &= \mathbf{G}(\boldsymbol{\theta})\mathbf{H}_M\mathbf{u} - (\boldsymbol{\nu}_{\theta c} - \boldsymbol{\eta}_{\theta l}) \end{aligned} \tag{19}$$

where

$$\boldsymbol{\eta}_{\rho l} = \mathbf{K}_1\dot{\boldsymbol{\rho}} + \mathbf{K}_2\boldsymbol{\rho}$$

$$\boldsymbol{\eta}_{\theta l} = \mathbf{f}(\boldsymbol{\theta},\dot{\boldsymbol{\theta}}) + \mathbf{K}_3\dot{\boldsymbol{\theta}} + \mathbf{K}_4\boldsymbol{\theta}$$

Defining state variables as $\mathbf{e}_\rho = [\boldsymbol{\epsilon}_\rho^\top \ \dot{\boldsymbol{\epsilon}}_\rho^\top]^\top$, $\mathbf{e}_\theta = [\boldsymbol{\epsilon}_\theta^\top \ \dot{\boldsymbol{\epsilon}}_\theta^\top]^\top$, and $\mathbf{e} = [\mathbf{e}_\rho \ \mathbf{e}_\theta]^\top$, Eq. (19) can be written in first order state space form as

$$\dot{\mathbf{e}} = \mathbf{A}_m\mathbf{e} + \mathbf{B}(\boldsymbol{\theta})(\mathbf{H}\mathbf{u} - \mathbf{w}) \tag{20}$$

with

$$\mathbf{A}_m = \begin{bmatrix} \mathbf{A}_{1m} & \mathbf{0}_{3\times3} \\ \mathbf{0}_{3\times3} & \mathbf{A}_{2m} \end{bmatrix}, \quad \mathbf{A}_{1m} = \begin{bmatrix} \mathbf{0}_{3\times3} & \mathbf{I}_{3\times3} \\ -\mathbf{K}_1 & -\mathbf{K}_2 \end{bmatrix},$$

$$\mathbf{A}_{2m} = \begin{bmatrix} \mathbf{0}_{3\times3} & \mathbf{I}_{3\times3} \\ -\mathbf{K}_3 & -\mathbf{K}_4 \end{bmatrix} \tag{21}$$

and

$$\mathbf{B}(\boldsymbol{\theta}) = \begin{bmatrix} \mathbf{0}_{3\times3} & \mathbf{0}_{3\times3} \\ \frac{1}{m}{}^L\mathbf{R}_S(\boldsymbol{\theta}) & \mathbf{0}_{3\times3} \\ \mathbf{0}_{3\times3} & \mathbf{0}_{3\times3} \\ \mathbf{0}_{3\times3} & \mathbf{G}(\boldsymbol{\theta}) \end{bmatrix}$$

$$\mathbf{w} = \begin{bmatrix} \mathbf{w}_F \\ \mathbf{w}_M \end{bmatrix} = \begin{bmatrix} m^S\mathbf{R}_L(\boldsymbol{\theta})(\boldsymbol{\nu}_{\rho c} - \boldsymbol{\eta}_{\rho l}) \\ \mathbf{G}^{-1}(\boldsymbol{\theta})(\boldsymbol{\nu}_{\theta c} - \boldsymbol{\eta}_{\theta l}) \end{bmatrix} \tag{22}$$

$\mathbf{K}_1$, $\mathbf{K}_2$, $\mathbf{K}_3$, and $\mathbf{K}_4$ are designed to be positive definite, $\mathbf{A}_{1m}$ and $\mathbf{A}_{2m}$ are Hurwitz and therefore, $\mathbf{A}$ is also Hurwitz. The term $\mathbf{w}$ can be thought of as the ideal controls for tracking the reference model Eq. (18) since if $\mathbf{H}\mathbf{u} = \mathbf{w}$ the system of Eq. (15), the tracking error goes exponentially to zero.

The controller was designed for the error system using the Lyapunov approach to control design. A Lyapunov function is used to design the controls such that the error equation (20) is asymptotically stable. To begin, the following candidate function is selected:

$$V(\mathbf{e}) = \mathbf{e}^\top\mathbf{P}\mathbf{e} \tag{23}$$

where $\mathbf{P} = \mathbf{P}^\top > 0$. Differentiating Eq. (23) with respect to time and using Eq. (20) results in the following Lyapunov derivative

$$\frac{dV}{dt} = \mathbf{e}^\top\left(\mathbf{A}_m^\top\mathbf{P} + \mathbf{P}\mathbf{A}_m\right)\mathbf{e} + 2\mathbf{e}^\top\mathbf{P}\mathbf{B}(\boldsymbol{\theta})(\mathbf{H}\mathbf{u} - \mathbf{w}) \tag{24}$$

Since $\mathbf{A}_m$ is Hurwitz, for every specified positive definite symmetric matrix $\mathbf{Q}$ there exists a unique positive definite symmetric matrix $\mathbf{P}$ that is a solution to the Lyapunov equation:

$$\mathbf{A}_m^\top\mathbf{P} + \mathbf{P}\mathbf{A}_m = -\mathbf{Q} \tag{25}$$

and if $2\mathbf{e}^\top\mathbf{P}\mathbf{B}((\boldsymbol{\theta}))(\mathbf{H}\mathbf{u} - \mathbf{w}) \le 0$, then Eq. (20) is asymptotically stable [24]. The only term that can be modified in Eq. (24) by the thruster values is the term

$$2\mathbf{e}^\top\mathbf{P}\mathbf{B}\mathbf{H}\mathbf{u} \tag{26}$$

Thus at each time step $\mathbf{u}$ is chosen such that expression (26) is negative. To accomplish this, let $\mathbf{a} = \mathbf{e}^\top\mathbf{P}\mathbf{B}\mathbf{H}$, then the components of $\mathbf{u}$ are computed as follows:

$$u_i = \begin{cases} u\left\lceil\dfrac{a_i - |a_i|}{2a_i}\right\rceil & \text{for } a_i \neq 0 \\ 0 & \text{for } a_i = 0 \end{cases} \quad \text{for } i = 1,\ldots,12 \tag{27}$$

This results in $u_i = 0$ or $u_i = u$, which designates the thruster being OFF or ON, respectively. An estimation of the Lyapunov derivative, Eq. (24), is calculated at each time step using previous values of the Lyapunov equation. Fuel can be saved by having the testbed not thrust when the Lyapunov derivative is already negative below a chosen threshold. This has the added effect of slowing down the movement towards the final position but does not cause instability since it still requires a negative Lyapunov derivative.

5. Testbed GNC experiments

5.1. Experiments

The 6DOF testbed hardware and GNC systems were tested by performing hardware-in-the-loop experiments. These experiments validate the ability of the testbed to accurately simulate complex spacecraft autonomous proximity maneuvers, which allows for the validation of novel GNC algorithms.

The experiments presented here consist of having the AS move to a target state from an initial state using the control generated from the Lyapunov-based thruster selection described in the previous section. In the experiments run so far on the testbed, the control has been used for regulation alone. In other words, starting from a given initial position and attitude, the AS is forced to reach a desired position and/or attitude without the path being specified (no guidance). These experiments corroborate the control strategy stability and assess the performance of the testbed.

5.2. Simulink model

MATLAB's Simulink is used to implement the control strategy as well as handle the navigation systems and control the thruster relays. The Simulink model, shown in Fig. 14, is used to generate C code, which can be compiled and run on the onboard Linux computer. The PC104 and a desktop computer, which runs MATLAB and Simulink, both use Real Time Application Interface (RTAI) Linux. The RTAI operating system was chosen because it allows the applications to run in real time without being interrupted by operating system tasks. Having the same operating system on the two computers allows executables generated on the desktop through the Simulink Coder to be transferred to, and run on, the PC104. The main blocks in the model are the Sensor Package, the State Estimator, Lyapunov Controller, and the Diamond Relay Board. The Sensor Package block contains the PhaseSpace System block created in the ADAMUS lab to communicate with the PhaseSpace server and to output the current position and attitude of the AS. This block also can be used in simulation via a global variable switch, which changes the block to use the Simulink Aerospace Blockset 6DOF dynamics

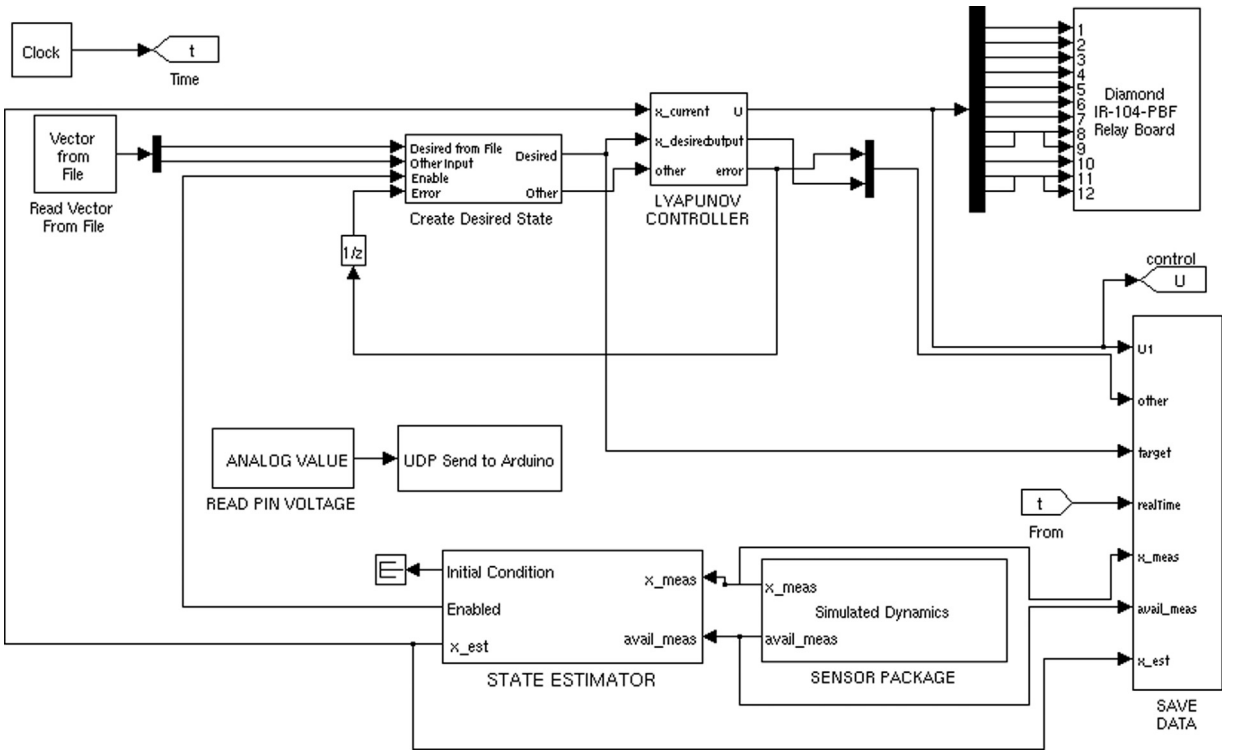

Fig. 14. Simulink model.

block to propagate the position and attitude. The State Estimator block contains a Kalman filter and extended Kalman filter which are used to estimate the position, velocity, attitude, and angular velocity information from the position and attitude information from the Phasespace data. The Lyapunov Controller block contains the implementation of the Lyapunov-based thruster selection, which is described in Section 4.2. The output of the Lyapunov Controller block is the 12×1 vector, which contains 1's for the thrusters which should be turned ON and 0's for the thrusters which should be kept or turned OFF. The Diamond Relay Board block operates the onboard relays using the output of the control block. The block Save Data collects the data held to be held in RAM until then end of an experiment when it is saved to an onboard flash hard drive. The data is taken from the hard drive back to a desktop computer running Linux and MATLAB so the data can be plotted and analyzed. The blocks associated with CD balancing can also be seen. The first block, called Read Pin Voltage, reads the pressure value from the A/D pin connected to the pressure transmitter. The next block, UDP Send to Arduino, continuously sends the pressure data to the Arduino over UDP.

5.3. Results

Experiments were run starting at an arbitrary initial condition with the testbed floating freely but not moving on the epoxy floor. The testbed software, represented in Fig. 14, was executed causing the testbed to regulate to a set of predetermined points. The results presented here show the testbed as it is regulated to a point near the center of the epoxy floor. Once all DOF were below the thresholds at once, the testbed then returned to its initial state, except for the vertical one, going only in one direction. A flowchart of the experiment can be seen in Fig. 15, while Table 4 summarizes the requirements for a successful test.

The change in target state can be seen in the experimental data shown in Fig. 16 at around 80 s. An exception was made for the vertical translation, which first regulated like the other DOF but then simply maintained its position for the return trip. The results for regulation in 6DOF are shown in Fig. 16 and can be seen in video online at url:http://www.riccardobevilacqua.com/multimedia.html, opening the video entitled "6 DOF (8 degrees attitude tolerance – "there and back")". The 8 degrees error tolerance on attitude was chosen via numerical simulations, as a satisfactory balance between thrusting effort and a final trajectory showing a successful maneuver. This procedure is an example of one of the most important benefits of ground based testbeds: being able to tune GNC via computer simulations, and then perform experimental validation to confirm their validity. The experiment demonstrates that along the three axes in position, the control was able to move from the initial state to the desired state then return to the initial state. The same can be seen in the Euler angles. The overshooting shown in some of the states could be reduced/increased in numerical simulations first, then new experiments could be run, once again showing the main goal of rapid prototyping of GNC algorithms and ground tests. The multimedia web page provided above shows additional tests performed with the ADAMUS simulator. Particularly, an additional experiment with 5 degrees attitude tolerance can be seen.

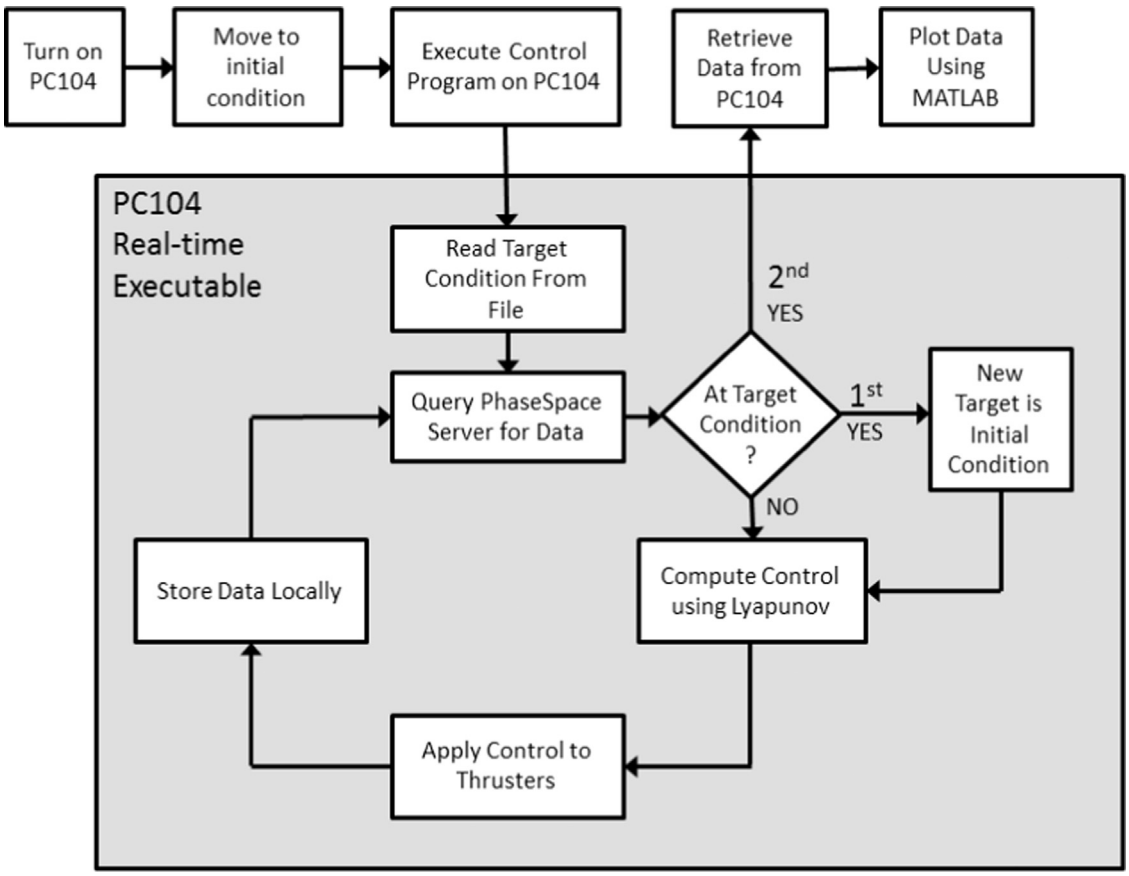

Fig. 15. Flowchart showing the steps performed when running an experiment.

Table 4
Requirements for the experiment.

State	Desired intermediate state	Desired final state	Desired accuracy
x	1500 mm	Random state at initial time	50 mm
y (vertical state)	1600 mm	1600 mm	50 mm
z	1500 mm	Random state at initial time	50 mm
θ_x	0 deg	Random state at initial time	8 deg
θ_y	−100 deg	Random state at initial time	8 deg
θ_z	0 deg	Random state at initial time	8 deg

The experiment also included a threshold for position and attitude, which allowed small errors to be ignored to reduce chatter at steady state. For position, this threshold was 5 cm and the effects cannot be seen in the plots in Fig. 16. For attitude, the threshold used was 8°. Euler angles θ_x and θ_z are close to or under this threshold for nearly the entire experiment, which can be seen in the movement to and from the goal line when under 8°. The movement under the threshold was not caused by the thrusters but instead caused by small imbalances in the AS.

The commanded signals to the thrusters are shown in Fig. 17.

The thrusters on the testbed are ON-OFF thrusters with a constant thrust force of .3 N per thruster. The density of the thrust profiles is largely affected by a threshold on the Lyapunov derivative, which determines whether thrust is currently necessary to decrease the error. Choosing a different threshold or the controller itself would greatly change the density and magnitudes of the thrust profiles. This experiment clearly shows the 6DOF capabilities of the testbed as it is able to move from an initial to a final condition in a controlled way in 6DOF.

5.4. Limitations and future work

There are a few aspects of the testbed vertical motion which either require improvement or represent limitations in design. Motion in the vertical direction appears to currently encounter more friction than the motion in the other two translational directions. This friction is mostly due to imperfections in the air bushing alignment, tube connections, and pulley cables; however, not all

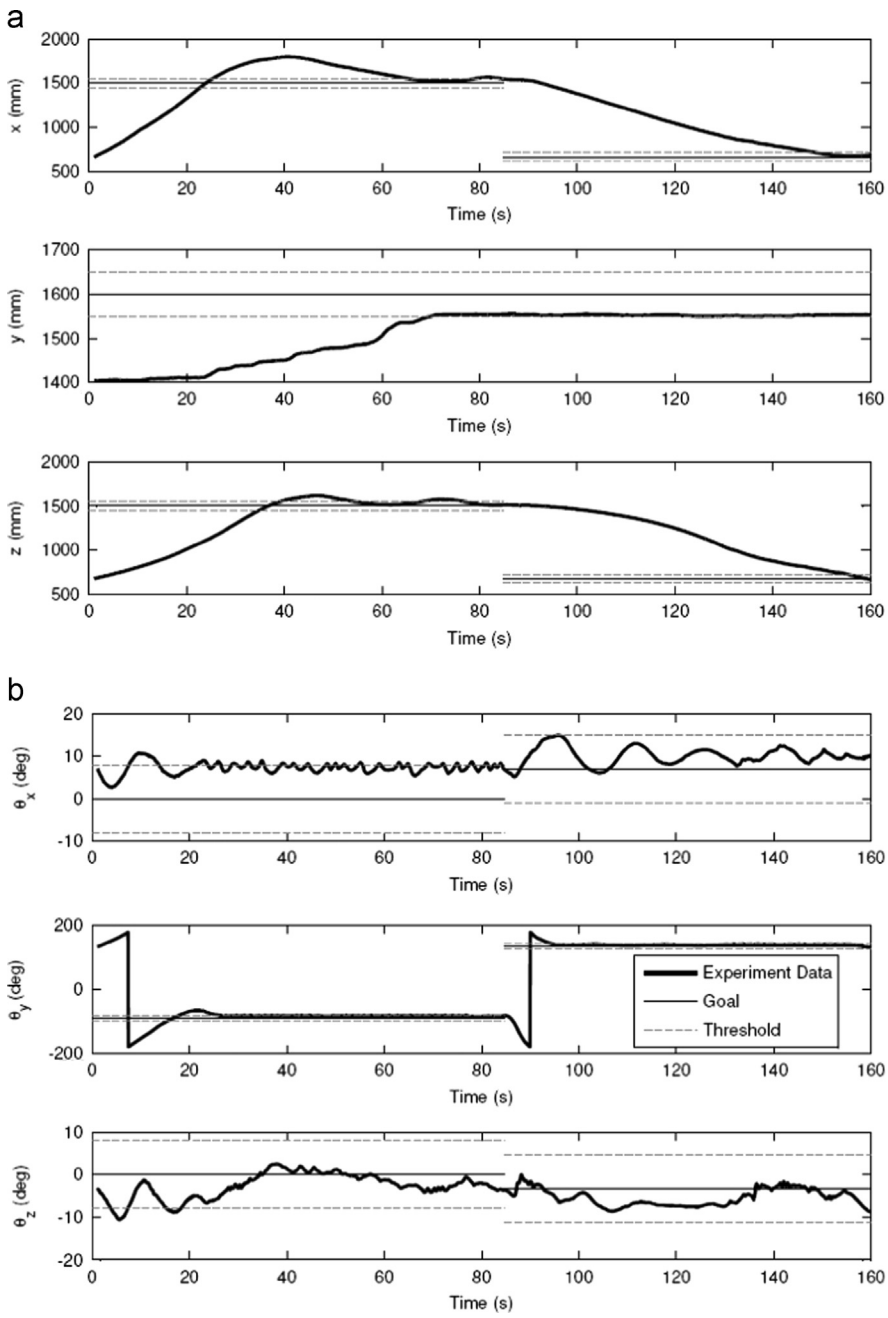

Fig. 16. 6 DOF Regulation Results. See also Table 4. (a) Position and (b) orientation.

vertical disturbances can be eliminated with the current design.

The largest disturbance is caused by the difference in mass between the vertical DOF and the two other translational DOF. The entire testbed must be moved when translating in either of the DOF along the epoxy floor. In contrast, AS motion in the vertical DOF involves the movement of only around 70% of the mass of the testbed - the counterbalance deck, AS, and supporting column. This difference in mass is an aspect of design, which cannot be eliminated with the counterbalance approach. The current control method was designed ignoring the difference in mass in the two DOF with no ill effects, thanks to its feedback nature. Future software may consider this difference in mass, and filter the thrust commands sent to the thrusters appropriately.

The second largest source of disturbance is found in the balancing of the AS and the balancing of the counterbalancing system. The AS balancing is currently done human-in-the-loop. However, the disturbances caused by

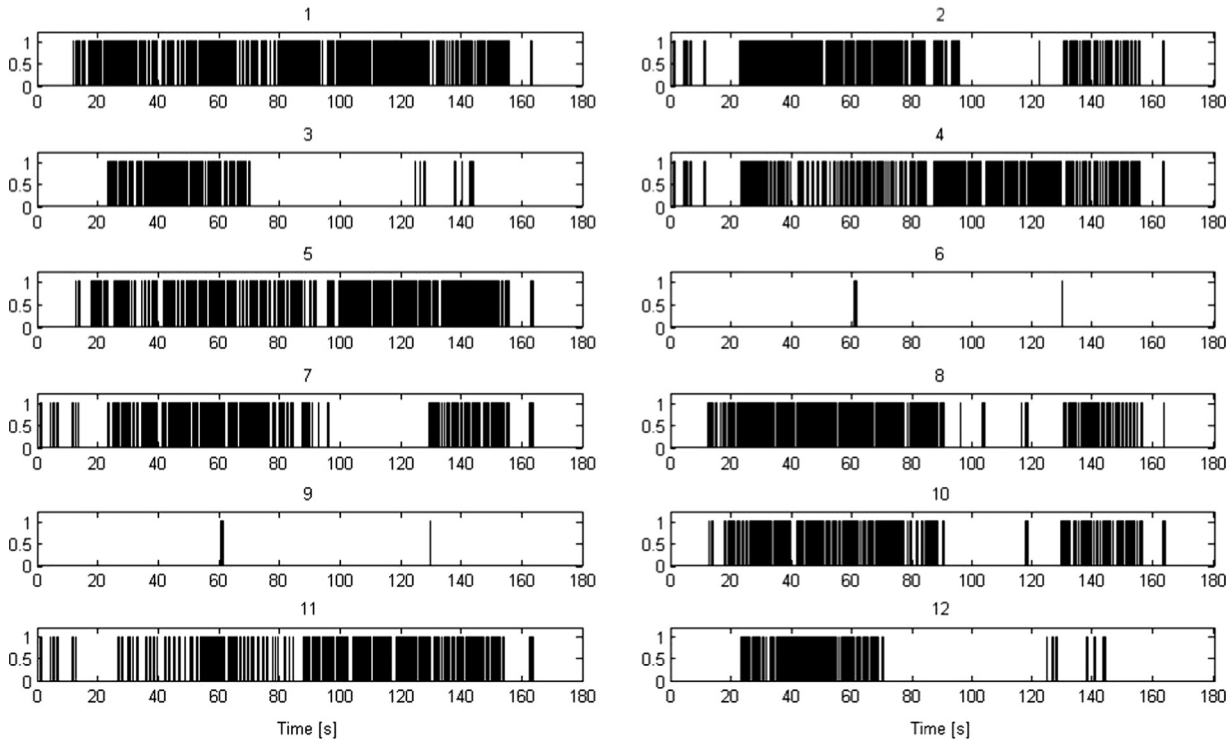

Fig. 17. Thrusters commands history. 1 indicates firing, 0 indicates thruster off.

the lack of alignment of the center of mass and the center of rotation are definitely within the ability of the controller to accommodate, as can be seen in the results of the testbed experiments. In the future, the balancing of the AS can be improved through adaptive balancing, which can remove human error and provide far more accurate results.

The counterbalancing system dynamic mass adjustment is currently done by measuring the pressures in the two AS tanks and maintaining the same pressure in the two CD tanks. It was desired that the balancing of pressures would correspond to a rough balancing of mass. With air being released in equal quantities, the two ends of the counterbalance would remain equal as air is released through the thrusters. The use of pressure difference to approximate mass difference is justified by the assumption that the two sets of tanks should be at roughly the same temperature as long as they are filled over the same time and release air at the same rate. This assumption was tested through an experiment where the AS was programmed to run through a GNC experiment using simulated dynamics. This caused the thrusters to release air in a fashion resembling that of an actual experiment, though over a much shorter time period. During this time the counterbalance deck released air to compensate for pressure differences in the same way it does for the experiments. After each thruster firing sequence, the TS and AS were weighed to measure the change in mass of both portions of the testbed. Since the only cause of change was the air released from both sets of tanks, this allowed for a direct measurement of the mass of air lost. As can be seen in Fig. 18, the mass released from the

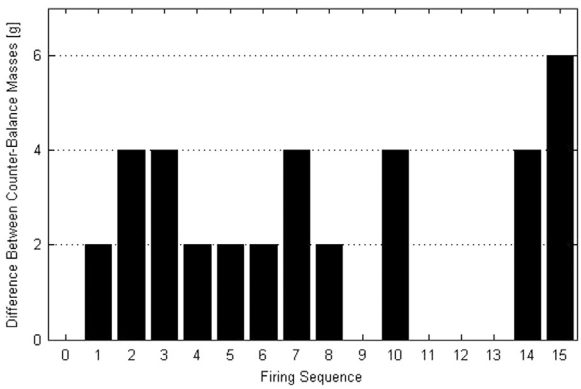

Fig. 18. Weight test: the difference in mass between the counterbalance platforms remains below 6 g as the thrusters are fired. Each firing sequence lasts 4 s, and the onboard software runs the code used for the experiment presented earlier in the paper.

counterbalancing deck follows closely the mass lost from the AS with a maximum difference of 6 g. With each thruster capable of providing .3N of force, the disturbance caused by 6 g difference in the counterbalance should be easily overcome by control forces. If a case is encountered where more precise balancing is required, the mass difference calculation would be improved by including temperature measurements of the tanks, along with the already measured pressure.

Lastly, the tubing running from the bottom deck of the TS platform to the counterbalancing deck to provide air for

the air bushings will cause some disturbance as the decks move relative to each other. Experiments to quantify the effect can be run, but the effect is expected to be minimal since the tubing can move freely.

The long term goal of the ADAMUS laboratory is to build multiple units and employ them for full 6DOF relative motion experiments, as the facility can accommodate several simulators.

6. Conclusion

The six degrees of freedom small spacecraft simulator testbed developed at the Advanced Autonomous Multiple Spacecraft laboratory is a unique platform, which reproduces all degrees of motion using air bearings. The experimental facility described herein is currently able to operate spacecraft weighing less than 10 kg and their algorithms in real time. In this work, the hardware and software details of the testbed have been presented, along with a Lyapunov-based thruster activation strategy, which was chosen to demonstrate the capability of the testbed to evaluate Guidance, Navigation, and Control algorithms. The experiment for validating the functions of the testbed and for assessing Guidance, Navigation, and Control algorithms with hardware-in-the-loop is described. The results of this experiment confirm the testbed's ability to move and be controlled in six degrees of freedom. Use of the testbed in validating the Lyapunov-based thruster selection control method demonstrates the utility of the testbed for the design and testing of Guidance, Navigation, and Control methodologies. Future work on the testbed will involve efforts to reduce the friction in the vertical translation as well as further experiments to quantify the disturbances caused by friction and balancing in the system. Future work will also include the implementation of balancing software for the Attitude Stage center of mass alignment with the center of rotation. This will allow the testbed to exhibit the desired dynamics more accurately.

Acknowledgements

This research was partially supported by the United States National Aeronautics and Space Administration (NASA), under a subcontract from the Satellite Servicing Capabilities Office (SSCO) at NASA Goddard Space Flight Center (subcontract of Grant no. NNX10AD17A).

References

[1] P. Thakker, W.A. Shiroma, Emergence of Pico- and Nanosatellites for Atmospheric Research and Technology Testing, American Institute of Aeronautics and Astronautics, Reston, VA, 2001.
[2] J.L. Schwartz, M.A. Peck, C.D. Hall, Historical review of air-bearing spacecraft simulators, J. Guidance Control Dyn. 26 (2003) 513–522, http://dx.doi.org/10.2514/2.5085.
[3] J. Masciarelli, J. Deppen, J. Bladt, J. Fleck, D. Lawson, Demonstration of an aerocapture GNC system through hardware-in-the- loop simulations, in: 33rd Annual AAS Guidance and Control Conference, Breckenridge, CO, 2010.
[4] J. Jung, S. Park, K.S., Y.H. Eun, Y. Chang, Hardware-in-the-loop simulations of spacecraft attitude synchronization using state-dependent riccati equation technique, Adv. Space Res. 51 (2013) 434–449. doi: http://dx.doi.org/10.1016/j.asr.2012.09.004.
[5] W.R. Wilson, M.A. Peck, An air-levitated testbed for flux pinning interactions at the nanosatellite scale, in: AIAA Modeling and Simulation Technologies Conference 2010, Washington, DC, 2010.
[6] D. Cho, D. Jung, P. Tsiotras, A 5-dof experimental platform for spacecraft rendezvous and docking, in: AIAA Infotech at Aerospace Conference and Exhibit and AIAA Unmanned...Unlimited Conference, Reston, VA, 2009.
[7] X. Jian, Y. Gang, B. and QinJun, L.J. Design and development of a 5-dof air-bearing spacecraft simulator, in: Proceedings—2009 International Asia Conference on Informatics in Control, Automation, and Robotics, CAR 2009, Piscataway, NJ, 2009, pp. 126–130.
[8] A. Ledebuhr, L. Ng, M. Jones, B. Wilson, R. Gaughan, E. Breitfeller, W. Taylor, J. Robinson, D.R. Antelman, D. Neilsen, Micro-satellite ground test vehicle for proximity and docking operations development, in: 2001 IEEE Aerospace Conference Proceedings, Piscataway, NJ, 2001, pp. 2493–2504.
[9] S.B. McCamish, M. Romano, S. Nolet, C.M. Edwards, D.W. Miller, Flight testing of multiple spacecraft control on spheres during close proximity operations, J. Spacecr. Rockets 46 (2009) 1202–1213.
[10] M. Kong, A. Saenz-Otero, S. Nolet, D.S. Berkovitz, D.W. Miller, S.W. Sell, Spheres as a formation flight algorithm development and validation test bed: Current progress and beyond, in: Proceedings of 2nd International Symposium on Formation Flying Missions and Technologies, Greenbelt, MD, 2004.
[11] M.W. Regehr, A.B. Acikmese, A. Ahmed, M. Aung, K.C. Clark, P. MacNeal, J. Shields, G. Singh, R. Bailey, C. Bushnell, A. Hicke, B. Lytle, R.E. Rasmussen, The formation control testbed, in: IEEE Aerospace Conference Proceedings, vol. 1, Piscataway, NJ, 2004, pp. 557–563.
[12] S.P. Viswanathan, A. Sanyal, L. Holguin, Dynamics and control of a six degrees of freedom ground simulator for autonomous rendezvous and proximity operation of spacecraft, in: AIAA Guidance, Navigation, and Control Conference 2012, Washington, DC, 2012.
[13] G. Guglieri, F. Maroglio, P. Pellegrino, L. Torre, Design and development of guidance navigation and control algorithms for spacecraft rendezvous and docking experimentation, Acta Astronaut. 94 (2014) 395–408.
[14] I. Kawano, M. Mokuno, T. Kasai, T. Suzuki, Result of autonomous rendezvous docking experiment of engineering test satellite-vii, J. Spacecr. Rockets 38 (2001) 105–111, http://dx.doi.org/10.2514/2.3661.
[15] M.R.D.A. Friedman, T.J. Shay, Laboratory experimentation of autonomous spacecraft approach and docking to a collaborative target, J. Spacecr. Rockets 44 (2007) 164–173, http://dx.doi.org/10.2514/1.22092.
[16] R. Bevilacqua, M. Romano, F. Curti, A. Caprari, V. Pellegrini, Guidance Navigation and Control for Autonomous Multiple Spacecraft Assembly: Analysis and Experimentation, International Journal of Aerospace Engineering 2011 (2011) 18, http://dx.doi.org/10.1155/2011/308245. (308245).
[17] G. Gaias, J.-S. Ardaens, S. D'Amico, Formation flying testbed at dlr's german space operations center (gsoc), in: 8th International ESA Conference on GNC (GNC 2011), Czech Republic, 2011.
[18] J.J. Kim, B.N. Agrawal, System identification and automatic mass balancing of ground-based three-axis spacecraft simulator, in: AIAA Guidance, Navigation, and Control Conference, Reston, VA, 2006, pp. 4224–4235.
[19] J.J. Kim, B.N. Agrawal, Automatic mass balancing of air-bearing-based three-axis rotational spacecraft simulator, J. Guidance Control Dyn. 32 (2009) 1005–1017, http://dx.doi.org/10.2514/1.34437.
[20] J. Snider, M. Plank, D. Lee, H. Poizner, Simultaneous neural and movement recording in large-scale immersive virtual environments, in: Biomedical Circuits and Systems Conference (BioCAS), San Diego, CA, 2011, pp. 98–101.
[21] C. Shake, K. Saulnier, R. Bevilacqua, Spacecraft attitude determination system using nano optical devices and linux software libraries, AIAA J. Aerosp. Comput. Inf. Commun. 10 (2013) 369–384, http://dx.doi.org/10.2514/1.I010049.
[22] F. Curti, M. Romano, R. Bevilacqua, Lyapunov-based thrusters' selection for spacecraft control: analysis and experimentation, J. Guidance Control Dyn. 33 (2010) 1143–1160, http://dx.doi.org/10.2514/1.47296.
[23] W.H. Clohessy, R.S. Wiltshire, Terminal guidance system for satellite rendezvous, J. Aerosp. Sci. 27 (1960) 653–658.
[24] H.K. Khalil, Nonlinear Systems, 3rd ed. Prentice-Hall, Upper Saddle River, NJ, 2002.

Kelsey Saulnier graduated with a Bachelor of Science in Computer Engineering from Rensselaer Polytechnic Institute in 2007. She began research in the ADAMUS lab as an undergraduate and continued her work there as a graduate student. Kelsey completed her Master of Science, also in Computer Engineering, in 2013. Her work at the ADAMUS lab focuses on the 6DOF testbed and control software.

David Pérez is a Postdoctoral Research Associate in the ADvanced Autonomous MUltiple Spacecraft (ADAMUS) Laboratory. Davids main research interests are Guidance, Navigation and Control of autonomous Spacecraft and Robotics. He received his B.Sc. (2008) in Mechanical Engineering from St. Cloud State University, St. Cloud, Minnesota and his M. Eng (2009) and Ph.D. (2013) in Mechanical Engineering and Aeronautical Engineering respectively from the Rensselaer Polytechnic Institute, Troy, New York.

Rosemary Huang is a native of Southern California. After graduating from Laguna Hills High School, she went on to attend the University of California, Berkeley, where she earned a Bachelor of Science degree in Mechanical Engineering in May of 2000. Following the completion of her undergraduate education, she continued her studies at Berkeley, earning a Master of Science degree, also in Mechanical Engineering, in August of 2003. She then moved to Indiana, to pursue a Ph.D. at Purdue University in West Lafayette. She completed her Doctorate in Aeronautical and Astronautical Engineering in 2012. Rosemary was the ADAMUS lab manager in 2013 and 2014.

Daniele Gallardo received his Ph.D. in Mechanical Engineering from Rensselaer Polytechnic Institute in 2014. Daniele holds a Bachelor and a Master Degree in Mechanical Engineering from the Politecnico di Torino, Italy. Daniele spent one year of his Master at the Massachusetts Institute of Technology as a research assistant where he developed his thesis related to PEM fuel cells degradation. The foci of Danieles Ph.D. research are the study of fluid–structure interactions and the development of novel mathematical models tailored for control purposes and based on reduced order modeling techniques. His current projects are related to vibration mitigation of airfoils and cross wind response of tall buildings.

Grace Tilton graduated from RPI in 2014 with a dual degree in aerospace and mechanical engineering. She has been a member of the ADAMUS lab since 2011, assisting with a variety of projects related to spacecraft simulation and design as well as participating in multiple varsity sports and Tau Beta Pi National Engineering Honor Society. She maintains a high level of academic success and these efforts have been recognized with the 2011 RPI Founders award and 2013 Barry Goldwater Scholarship.

Riccardo Bevilacqua is an associate professor of the Mechanical and Aerospace Engineering Department at the University of Florida. He holds a M.Sc. in Aerospace Engineering (2002), and a Ph.D. in Applied Mathematics (2007), both earned at the University of Rome, “Sapienza”, Italy. He was a US National Research Council post doctoral fellow from 2007 to 2010, and an assistant professor at RPI before joining University of Florida. He also worked as a project engineer in Mission Analysis at Grupo Mecanica del Vuelo in Madrid, Spain, during 2003. Dr. Bevilacqua's research interests focus on Guidance, Navigation, and Control of multiple spacecraft systems and multiple robot systems.